Published in final edited form as:
Anal Chem. 2010 September 1; 82(17): 7227–7236. doi:10.1021/ac101003f.

Multiplexed NMR: An Automated CapNMR Dual-Sample Probe

James A. Norcross[†], **Craig T. Milling**[†], **Dean L. Olson**[†], **Duanxiang Xu**[†], **Anthony Audrieth**[†], **Robert Albrecht**[†], **Ke Ruan**[§], **John Likos**[§], **Claude Jones**[§], and **Timothy L. Peck**[*,†]

[†] Protasis/MRM Corporation, 101 West Tomaras Avenue, Savoy, Illinois 61874

[§] Pfizer Corporation, 700 Chesterfield Parkway West., Chesterfield, MO 63017

Abstract

A new generation of micro-scale, nuclear magnetic resonance (CapNMR™) probe technology employs two independent detection elements to accommodate two samples simultaneously. Each detection element in the Dual-Sample CapNMR Probe (DSP) delivers the same spectral resolution and S/N as in a CapNMR probe configured to accommodate one sample at a time. A high degree of electrical isolation allows the DSP to be used in a variety of data acquisition modes. Both samples are shimmed simultaneously to achieve high spectral resolution for simultaneous data acquisition, or alternatively, a flowcell-specific shim set is readily called via spectrometer subroutines to enable acquisition from one sample while the other is being loaded. An automation system accommodates loading of two samples via dual injection ports on an autosampler and two completely independent flowpaths leading to dedicated flowcells in the DSP probe.

Keywords

NMR; Microcoil; Multicoil; CapNMR; Dual-Sample; Dual-Flowcell

Nuclear magnetic resonance (NMR) spectroscopy has distinguished itself as an exemplary method for the elucidation of chemical structure, determination of chemical purity, and quantitation.[1] However, a multiple order-of-magnitude inferiority in mass sensitivity relative to other well-known chemical detectors[2,3] has constrained the role of NMR, which is sometimes precluded in applications due simply to the amount of sample required and the amount of experimental time necessary to attain sufficient signal-to-noise ratio (S/N). Recent advances in the higher strength and smaller footprint of shielded superconducting magnets, the development of detection probes with enhanced sensitivity, and the emergence of new generations of NMR-inclusive chemometric methods[4–6] and spectral identification algorithms[7–9] have elevated the role of NMR as complementary tool for modern pharmaceutical analysis.

THEORETICAL BASIS

Dual-Sample Probe

Microcoil-based probes provide a nearly 10-fold enhancement in mass-sensitivity relative to conventional 5 mm tube probes.[10,11] In general, smaller-volume samples are easier to shim, and for the purpose of this specific effort, more than one small sample can fit into the fixed homogeneous (typically 1 cm diameter spherical volume, DSV) region of a conventional superconducting magnet. Previous academic efforts using multi-sample, microcoil-based probes have reported detection volumes ranging from low nanoliters to tens of microliters, and

[*]To whom correspondence should be addressed. tpeck@microNMR.com.

have involved a variety of geometrical configurations intended to address objectives ranging from diminished RF coupling to an ability to spatially encode using an applied magnetic field gradient.[12–23] The present report does not aim to provide comprehensive review of, or comparison to these approaches. This report describes the first commercial version of dual sample probe for high resolution NMR analysis. A volume of 10 μL is employed for each flowcell, with an observe volume (for RF detection) of 5 μL. These volumes represent a concentration generally well below the concentration limit when diluting tens or low hundreds of micrograms of a small molecule compound, typical of the mass obtained from analytical-scale (4.6 mm column i.d.) liquid chromatography separations or the volumes of aliquots available in modern pharmaceutical repositories.

Shown in Figure 1, the Dual-Sample Probe incorporates two flowcells stacked vertically. Both samples have dedicated RF microcoils and gradient coils, and both samples reside within a 1 cm DSV. The independent analysis of two samples and operation of two detection coils and circuits in the confined space of the NMR probe requires a high degree of magnetic and electrical isolation. Magnetic isolation involves strategic geometric arrangement of materials and careful manipulation of magnetic susceptibility so as to maintain (B_0) field homogeneity and NMR spectral resolution. Electrical isolation involves both static (gradient coil) and radiofrequency (detection coil) field components. Electrical isolation is addressed through geometric arrangement, as well as through ancillary shielding. While each of the magnetic and electrical isolation terms must be carefully addressed, the reduced size scale of the CapNMR regime provides additional advantage in terms of electrical decoupling. The most significant technical challenge involves RF electrical coupling between the two microcoils. Use of RF shielding must be accomplished in a manner that does not significantly diminish S/N or degrade spectral resolution.

NMR provides a unique perspective for measurement of RF electrical isolation to complement benchtop (electrical) network analysis. In the case of network analysis, coupling is measured simply as the RF energy delivered to one microcoil and sensed by a second microcoil in spatial proximity. Symmetry applies, and the reverse situation (where the original receiving coil transmits and the original transmitting coil receives) results in the same value of RF electrical coupling. Four proton coupling terms can be measured for each microcoil using NMR. The situation is illustrated in Figure 2, where the coupling source voltages are labeled FID_{xyz}. The subscripts xyz correspond to a free induction decay (FID) signal produced by sample x, originating from RF energy delivered to microcoil y, and received by microcoil z. A coupling coefficient F_{xyz} is subsequently defined normalized to the full strength FID_{xyz} produced from a 90° pulse applied and received by a coil surrounding a given sample. It's assumed that the two coils in the present design are electrically equivalent. However, it is instructive to note that coupling manifests differently in transmit and receive modes. In receive mode, the magnitude of signal received by a first coil due to magnetization of a second sample residing in a second coil and energized by that second coil is linearly related to the level of coupling. For example, a 2% coupling of the upper coil to the lower sample will result in a 2% error signal in the spectrum of the upper coil, where error is defined relative to the full-strength signal magnitude from the lower sample and assumes identical coils. In contrast, transmit coupling effects are non-linear, due to the sine function describing the tip angle vs. excitation power. In transmit mode, a 2% coupling of the upper coil to the lower sample will result in a tip angle of 2% of 90 degrees, i.e. 1.8 degrees, to the lower sample. The resulting S/N received in the lower coil is approximately sin(1.8)/sin(90) = 3% of the maximum value. The specific case of FIDs produced at the terminals of microcoil #2 is considered below.

FID_{222}—This self-coupling source term pertains to the most familiar form of excitation and detection, where sample #2 is excited by RF energy delivered to microcoil #2, with a FID measured at the terminals of microcoil #2.

FID_{212}—Appropriate receiver blanking can ensure that transmit energy applied to microcoil #1 is not directly detected by microcoil #2. However, energy in the form of stray B_1 field from microcoil #1 partially excites the spin system of sample #2. The magnetization of sample #2 is then available to be received as an FID at the terminals of microcoil #2. This error signal represents a quantitation error in the spectrum and S/N of sample #2.

FID_{112}—RF energy applied to microcoil #1 excites the spin system of sample #1. The decay in magnetization of sample #1 is weakly sensed by (the fringe field of) microcoil #2 and induces a FID (with chemical signature of sample #1) at the terminals of microcoil #2. This error signal represents an impurity in the spectrum of sample #2.

FID_{122}—Following the logic of FID_{212}, RF energy delivered to microcoil #2 will (though the stray B_1 field of microcoil #2) slightly perturb the spin system of Sample #1. Not only is a FID from Sample #1 received at the terminals of microcoil #1, but also, albeit very weakly, at the terminals of microcoil #2. In essence, the same fringe field of microcoil #2 is available to both partially excite and weakly receive Sample #1. The result is an impurity in the spectrum of sample #2. Since FID_{122} involves stray field coupling for both transmit and receive cycles, it is the weakest of the coupling source terms shown in Figure 2.

Incorporating geometric symmetry, the normalized coupling coefficients F_{xyz} are therefore given as:

$$F_{111}=FID_{111}/FID_{111}=F_{222}=FID_{222}/FID_{222}=1=0\,dB$$
$$F_{221}=FID_{221}/FID_{111}=F_{112}=FID_{112}/FID_{222}$$
$$F_{121}=FID_{121}/FID_{111}=F_{212}=FID_{212}/FID_{222}$$
$$F_{211}=FID_{211}/FID_{111}=F_{122}=FID_{122}/FID_{222}$$

Dual Sample Automation Configuration

Figure 3 represents one example of an analytical workflow that includes NMR for analyte characterization. For instance, modern MS-directed isolation strategies combine the power of rapid upstream MS characterization with information-rich NMR analysis of high-value analytes.[4] Direct analysis of chromatography fractions (typically micrograms of mass at analytical-scale) is often facilitated using vacuum centrifugation followed by reconstitution in a solvent of choice, including the option for deuterated solvent. The ability to employ valuable NMR data earlier in the analytical process (i.e., without the need to scale-up for greater mass) results in considerable cost- and time-savings.[24] The specific NMR configuration chosen to support the Dual-Sample Probe is illustrated in Figure 4. Sample submission is accomplished using dual injection valves (with dedicated sample transfer lines leading separately to each of two flowcells) residing on an autosampler and using chromatography-grade fluidic components. A web-based instrument controller coordinates sample loading, NMR data acquisition, and automated decision-making.

While modern NMR spectrometers accept multiple receiver channels, standard configurations typically employ a single receiver each for detection of low-frequency (X) nuclei and for detection of high-frequency (proton range) nuclei. A single set of gradient control circuits and amplifiers is also standard. To economically and efficiently accommodate these standard configurations, a multiplexed approach has been described to interface multi-sample probes to conventional NMR spectrometers.[17]

A multiplexing signal router (MSR, see Figure 4) was designed and built to interface the Dual-Sample Probe to the spectrometer previously described. A block diagram of the MSR is shown in Figure 5. Proton and carbon transmit signals are routed via radio frequency switches to the

appropriate (sample 1 or sample 2) preamplifier module. The FID passes first through the preamplifier (to preserve S/N) and is then routed to the receiver of the spectrometer via radio frequency switches that are included as part of the MSR design. The states of the RF switches are controlled using digital (TTL) lines accessible via the pulse sequence program and available on commercial spectrometers. Magnetic field gradient signals are routed through the MSR to the probe using a similar series of switches.

Acquisition Modes

The opportunity to acquire NMR signals from two distinct samples and detection circuits offers a range of operational possibilities. *Sequential acquisition* (Figure 6(a)) describes a mode where NMR data are acquired from sample #1 that was loaded into flowcell #1. During the first sequence period, flowcell #2 can be rinsed with solvent to prepare for subsequent loading of sample #2. In sequence period #2, NMR data is subsequently acquired from sample #2 while the first flowcell is rinsed with solvent and a new sample is loaded into flowcell #1. Typically five flowcell rinse volumes are recommended between samples to minimize sample-to-sample carry-over, requiring approximately 1 minute of time at standard flow rates. Conversely, *simultaneous acquisition* (Figure 6(b)) describes a mode where both samples are loaded prior to the start of NMR data acquisition, and where identical experiments are conducted on each sample. NMR data is acquired simultaneously from both samples. Simultaneous acquisition requires that the NMR spectrometer be equipped with dual receivers. Alternatively (and more cost-effectively) a multiplexed approach to signal acquisition can be employed, using the multiplexing signal router previously described (Figure 5) for routing of the transmitted and received signals. Illustrated in Figure 6(c), the multiplexed mode of acquisition takes advantage of the T_1 relaxation time of NMR samples. The speed of modern electronics is sufficient for managing multiplexed simultaneous experiments from multiple samples. Sample T_1 values range from milliseconds to seconds, whereas electronic switching times of microseconds are readily achieved. Further, modern spectrometers are capable of executing implicit acquisition statements embedded within the NMR pulse sequence, and of partitioning the acquired data into formats that can be fully differentiated as part of post-processing.

Sequential mode acquisition allows independent shimming of the individual samples. Each of the two shim settings is stored in a look-up table and called as part of the acquisition sequence for the appropriate sample. Multiple solvent conditions are similarly accommodated. In the case of simultaneous and multiplexed modes of acquisition, the two samples are shimmed concurrently, since field homogeneity is simultaneously required for both samples being analyzed.

Pulse Sequences for Multiplexed Signal Acquisition

Modification of the NMR pulse sequences to enable multiplexed signal acquisition from dual samples is illustrated in Figure 7 for the case of simple 1D proton acquisition, and in Figure S2 of the Supporting Information for representative two-dimensional homonuclear and heteronuclear data acquisitions. Shown in Figure 7, the modification of a 1D ^{1}H experiment to accommodate dual samples is accomplished by modifying the typical relaxation delay time (d1) of sample #1 to accommodate signal acquisition in sample #2 during this period of (otherwise unutilized) time. Implicit acquisition statements are embedded along with TTL control line code in the pulse sequence to instruct the NMR spectrometer concerning data storage from each sample and for maintaining correct timing for the acquisitions from both samples.

EXPERIMENTAL

A 600 MHz Dual-Sample Probe configured for $^{1}H\{^{13}C\}$ detection was delivered for evaluation in a pharmaceutical setting. The probe employs two horizontally-oriented (transverse to B_0), 10 μL-volume flowcells. Both microcoil circuits were impedance-matched to 50 ohms at ^{1}H and ^{13}C frequencies, and each circuit included a z-directed magnetic field gradient coil. A single ^{2}H lock was included on the lower detection circuit. A Protasis One-Minute NMR automation system was modified as illustrated in Figure 4 to include two independently controlled sample injection ports on the liquid handler. The system software was modified to separately track and monitor two independent samples from the point of sample loading through data acquisition and return of both samples to designated wellplate or microvial locations. All NMR measurements were performed using a Varian Inova spectrometer operating at 600 MHz ^{1}H frequency (14.1 T) and running VNMRJ software.

NMR performance assessment was accomplished using 5% $CHCl_3$ in DMSO-d_6 and 10 mM sucrose in DMSO-d_6 samples for homonuclear studies, and using 10 mM sucrose and 30 mM quinine in DMSO-d_6 in heteronuclear studies. Isolation measurements primarily involved 5% $CHCl_3$ in DMSO-d_6 and 100% acetone-d_6. Both flowcells were overfilled in the series of measurements described, as the removal of performance factors relating to sample loading most directly facilitates the objective of quantitative comparison of Dual-Sample Probe performance to that of a standard (single-sample) CapNMR probe of identical size. Details concerning optimization of fluidic performance and sample loading efficiency in 5 μL and 10 μL volume flowcells have been developed to a point of maturity over the past ten years, and are not reiterated here.[11]

Performance assessment of the DSP in one NMR application involved large scale, high throughput structure verification studies. In a pharmaceutical drug discovery environment, it is of great interest to confirm whether a proposed structure is consistent with the associated NMR spectra. Such verifications must be accomplished in a high throughput manner, with high accuracy. The DSP was employed in multiplexed acquisition mode using the Varian Inova spectrometer previously described. A modified pulse sequence library was created that included the 1-D proton, sensitivity-enhanced HSQC, and the Hadamard TOCSY. This trio of experiments was applied to each sample, with an achieved throughput of 100 samples/day. A report on the use of the Hadamard TOCSY in verification studies is planned for subsequent journal submission, and hence the details of the procedure will not be described here. Briefly, the protocol involved:

1. A predicted TOCSY spectrum is generated using the 2J, 3J and conjugated 4J 1H-1H couplings of a proposed structure.
2. 1H and HSQC NMR data are acquired using the DSP.
3. Combined 1H/HSQC verification is applied to obtain proton assignments.
4. The TOCSY constructed based on coupling predictions is mapped to the experimental TOCSY spectrum
5. Connectivity inconsistency between the predicted and experimental TOCSY results in a negative score for structure verification.

This approach is illustrated in Figure 8.

RESULTS

Sequential Shimming

Using $CHCl_3$ in both flowcells, spectral linewidths of 0.45/6.6/11.7 Hz and 0.59/6.6/10.8 Hz (0.11/0.55/50 % of maximum values of the proton peak) were obtained for the upper and lower samples, respectively. These spectra are provided in Figure S1 of the Supporting Information pertaining to this journal article. Both resolution measurements were made using the Varian res command and adjustment of only 6 shims (z1, z2, x, y, xy, and r2) relative to the values stored on the spectrometer for a room-temperature (RT) 5 mm tube probe. The data clearly demonstrate clean spectral baselines and artifact-free, symmetric peaks.

Both flowcells were subsequently rinsed and filled with sucrose. Proton 90 - degree pulse widths were separately determined to be 7.7 μs for both samples using a tpwr (proton RF transmit amplifier) setting of 40 and a 100 W amplifier, and ^{13}C 90 degree pulse widths were determined to be 4 μs for both samples using a pwx1v1 (carbon RF transmit amplifier) value of 40 and a 300 W amplifier. The single-scan S/N was measured on the highest-field doublet (~ 5.22 ppm) of the sucrose samples were 55 for the upper sample and 53 for the lower sample, using a noise bandwidth of 100 Hz, line broadening value of 0.7 Hz, and a noise referenced region of 6–9 ppm. Spectra are provided in Figure S3 of the Supporting Information.

The multiplexing signal router was inserted into the transceiver chain as shown in Figure 4. Subsequent measurement of 90 – degree pulse widths resulted in 5.8 μs (upper sample) and 5.6 μs (lower sample) for ^{1}H using tpwr = 45, and 4.5 μs for ^{13}C for each sample using pwx1vl = 40. Gradient profile tests revealed maximum gradient strengths of 58 G/cm and 63 G/cm for the upper and lower coils, respectively.

Simultaneous Shimming

To evaluate the spectral resolution achievable by simultaneous shimming, both flowcells were rinsed and refilled with 5% $CHCl_3$. Spectral linewidth values of 0.63/6.9/12.7 Hz and 0.74/6.5/9.1 Hz were recorded for upper and lower samples, respectively. Simultaneous shimming involved adjustment of 11 of the 28 shim orders (z1, z2, z3, x, y, xz, yz, xy, r2, zxy, and zr2) relative to RT 5 mm probe values described above. The resulting NMR spectra are provided in Figure S4 of the Supporting Information. As before, good peak symmetry and clean spectral baselines are observed.

Both flowcells were rinsed and filled with 10 mM sucrose for assessment of S/N in multiplexed mode. The single-scan S/N of the anomeric peaks was 50 and 54 in the upper and lower samples, respectively for the same noise bandwidth and line broadening used previously. These data are shown in Figure S5 of the Supporting Information.

Ease of Use

A practical attribute of small-volume, room-temperature microcoil-based probes is that the probe can readily be removed from a magnet and re-installed with minimal effort. This translates to greater application diversity for the NMR magnet and spectrometer. To evaluate this aspect of probe functionality, the Dual-Sample Probe was removed from the magnet and a different probe employed for a period of approximately one week, after which the Dual-Sample Probe was re-inserted for a second evaluation. The height of the probe in the magnet was maintained at the previously established value via the mounting plate at the probe base. The previous shim file pertaining to simultaneous shimming was recalled without alteration. The $CHCl_3$ resolution standard was again employed in both flowcells for assessment of resolution. Linewidth values of 1.1/9/15 Hz or better were recorded for both samples without reshimming.

Isolation

Radio frequency electrical isolation between the two detection circuits in the probe was first measured using network analysis (Hewlett Package 4396B network analyzer, 85046A s-parameter test set). The isolation between the two microcoil circuits was greater than 30dB at 600 MHz (proton frequency) and greater than 35dB at 150 MHz (carbon frequency).

NMR-based isolation measurements were subsequently performed to assess proton isolation. A 5% $CHCl_3$ sample (#1) was employed in the upper flowcell (#1), and unless otherwise noted below, the lower flowcell (#2) contained 100% acetone-d_6 (sample #2). Different samples were purposely chosen to differentiate signal origins via chemical shifts.

FID_{111}—A 90 degree excitation pulse applied to the upper microcoil resulted in a single-scan S/N = 5610 for the FID from the upper sample induced in the upper microcoil. Therefore, FID_{111} = 5610

FID_{112}—The upper sample was fully excited using a 90 degree hard pulse delivered to the upper microcoil. Due to coupling, magnetization of the upper sample induced a small but measurable voltage in the lower microcoil. The S/N of the $CHCl_3$ peak measured in the spectrum received by the lower microcoil was 86 (86/5610 = 1.5 %).

FID_{121}—An excitation pulse delivered to the lower microcoil partially excites the upper sample. The S/N of the $CHCl_3$ peak measured in the spectrum received by the upper microcoil was 180.

FID_{122}—For this assessment the lower flowcell was evacuated of acetone and filled with 10 mM sucrose in DMSO-d_6. A 90 degree RF pulse was delivered to the sucrose sample by the lower microcoil. Coincidentally, the upper sample experienced a diminished but non-zero excitation angle. Subsequently, the magnetization of the upper sample is weakly received by the lower microcoil. The NMR spectrum of the lower microcoil is provided in Figure S6 of the Supporting Information section, and supports theoretical predictions of negligible F_{122} coupling. Results were not quantified.

Heteronuclear Experiments

The upper and lower flowcells were filled with 10 mM sucrose and 30 mM quinine, respectively, as described in the Experimental section. Multiplexed signal acquisition was performed using three pulse sequences modified for Dual-Sample Probe operation (Figures 6 and S1):

1. Dual 1-D proton (^1H) spectra,
2. Dual gradient-based homonuclear correlation (g-COSY) spectra,
3. Dual gradient-based, sensitivity-enhanced heteronuclear quantum coherence (g-HSQC) spectra.

The resulting NMR spectra shown in Figure 9 were obtained in 1 min, 7 s, 6 min, 6 s, and 28 min, 48 s for pairs (one each from two different samples) of ^1H, g-COSY, and g-HSQC spectra, respectively.

High Throughput Structure Verification Studies

A Hadamard-inclusive approach to connectivity-assisted structure verification was initially applied to a set of 41 representative pharmaceutical compounds, to assess the merit of this approach over ^1H/HSQC verification approaches where the Hadamard TOCSY is not included. The additional time necessary for inclusion of the Hadamard TOCSY in the suite of three NMR

experiments was less than the factor-of-two time savings achieved using the DSP for multiplexed processing of two samples simultaneously. The algorithmic benefit was considerable, and demonstrated a particularly enhanced capability to distinguish false positive results in the differentiation of structurally similar byproducts. Using only conventional ^{1}H/HSQC NMR data, 22% false positive results were reported, i.e., 9 of the 41 samples reported false positive. Using the ^{1}H/HSQC/Hadamard approach described above, the false positive rate dropped to 10%, i.e., only 4 samples. These details are being prepared for subsequent publication.

DISCUSSION

Isolation

Coupling coefficients are computed in Table 1. The assumption of identical coils yields a normalization of FID_{111} = 5610 for the $CHCl_3$ sample. Calculations are briefly outlined below:

F_{112} = 86/5610 = 1.5% = 20log(86/5610) = −36 dB, within a factor of 2 in signal magnitude when compared to the isolation value of 30 dB measured by network analysis.

F_{121}—The effective flip angle experienced by the spins in the upper sample by 90-degree excitation of the lower sample by the lower coil can be crudely estimated using the previously measured coupling coefficient, F_{112}. A net excitation of (1.5%)(90°) = 1.4° for the upper sample, with predicted S/N = [sin(1.4°)/sin(90°)]*5610 = 140. The measured value was S/N = 180, and suggests a 2% (−34 dB) coupling and 1.8° tip angle. Geometric symmetry would require that these two values be equal. The 0.5 % difference in F_{112} and F_{121} was not investigated further.

F_{122}—Based upon the previous measurements of F_{112} and F_{121}, the estimated value for F_{122} is approximately (2% × 2%) = 0.040% = −68 dB. The goal of the measurement represented by Figure S6 of the Supporting Information is not to accurately quantitate the value of −68 dB, but rather to simply demonstrate that it is of substantially lower magnitude than the other coupling coefficients and therefore negligible in most cases.

The receiver is connected to only one of the two microcoils at any one time when using the multiplexed mode of data acquisition (Figure 6(c)). Therefore, FIDs generated via the coupling terms FID_{112}, FID_{221}, FID_{121}, and FID_{212} are not received by the NMR spectrometer. The minor perturbation to sample magnetization due to these coupling coefficients has decayed significantly by the time that the multiplexer connects the receiver to the coil necessary for signal detection. Therefore, the effects of coupling coefficients FID_{112}, FID_{221}, FID_{121}, and FID_{212} can be neglected when using multiplexed operation. This leaves only the weakest coupling terms, FID_{122} and FID_{211}, as potential sources of unwanted signal contamination in this mode of acquisition.

In summary, the level of isolation provided by the Dual-Sample Probe enables a wide array of high throughput characterization studies. The multiplexed mode may be preferred over simultaneous mode operation in impurity analyses where the goal is characterization of low-abundance analytes in the ~ 1% or less range. When absolute isolation is required, the Dual-Sample Probe can be used in a sequential acquisition mode.

Spectral Resolution and S/N

Measured proton 90° pulse widths of 7.7 μs (tpwr = 40, 100 W amplifier, 0.5 W of ^{1}H transmit power) are approximately 15% greater than the pulse widths obtained using a single sample CapNMR probe of the same flowcell size on the same spectrometer and under identical

acquisition conditions. Similarly, the S/N values (anomeric proton, 10 mM sucrose) of 55 and 53 measured on the Dual-Sample Probe for the upper and lower flowcells, respectively, are 15% lower than values expected using a single sample CapNMR probe. Subsequent insertion of the multiplexing signal router (approximately 1 dB rated insertion loss) predicts a reduction in the power reaching the probe by a factor of 4/5, from 0.5 W to 0.4 W. Since B_1 field increases and 90° pulse width decreases as the square root of P, the pulse widths should increase by approximately $(5/4)^{½} \sim 12\%$ to 8.6 μsec. However, source power was simultaneously increased by approximately 3-fold (tpwr = 45, 100 W amplifier, 1.5 W of ^{1}H transmit power) in this experiment, resulting in (1.5 W)*(4/5) = 1.2 W reaching the RF coils. Therefore, a predicted net *decrease* in pulse width of $(0.5/1.2)^{½} = 65\%$ to a value of of (65% × 7.7 μs) = 5 μs is expected. As shown in the experimental section, measured values were 5.8 μs and 5.6 μs, suggesting an insertion loss of approximately 2 dB at proton frequency. For a fixed input power, this corresponds to longer pulse widths by 25 – 30 %. However, since during the receive portion of the acquisition sequence the pre-amplifier is located upstream of the MSR, a longer transmit pulse width does not imply a lower S/N during signal reception.

The ^{13}C 90 degree pulse widths measured with and without the MSR configuration were 4.5 μs and 4.0 μs, respectively; pwx1vl was set to 40. The measured increase of 0.5 μs (with MSR included) compares nearly exactly with the pulse width predicted from a 1 dB insertion loss and (4/5) scaling in signal power, i.e. a pulse width *increase* to 4 μs × $(5/4)^{½}$ = 4.5 μs.

The resolution and performance illustrated in the combined datasets of Figure 9 strongly demonstrate a new role that NMR can take alongside other analytical detection modalities for multiplexed sample analysis. Two detectors can be simultaneously shimmed for the purpose of ultra high throughput characterization, screening, and library-building. Alternatively, shims can be optimized to accommodate two different solvents, thereby eliminating the time required for changeover of the flowpath from one solvent to another. A third scenario involves separate optimization for different nuclei, e.g. with the top circuit tuned to $^{1}H\{^{13}C\}$ and the bottom circuit tuned for $^{1}H\{^{15}N\}$, or with the top circuit optimized for proton and the bottom circuit optimized for direct-detection of a second nucleus. Though not explained here, different flowcell volumes can be employed, e.g. where a top flowcell of minimum volume is optimized for highest mass-sensitivity, where a bottom flowcell of larger volume is designed to accommodate concentration-limited samples, or samples available in larger amounts. Flowcells can be assigned to specific tasks or specific groups, where each of two research groups want separate access to and responsibility for their own detector, or where institutional regulatory requirements make it practical to have one flowcell dedicated to specific protocols and samples, with a second flowcell available for open access or walk-up applications. Constraints with regard to timing in the pulse sequence program can usually be accommodated in a manner that provides performance and functional advantage relative to a one-sample-at-a-time configuration, which the Dual-Sample Probe does not preclude.

Looking forward to more than two multiplexed samples, Figures 6 and S1 indicate that a practical limit exists to the number of excitation and receive time periods (pw + at for Varian; p1 + aq for Bruker) that fit into a d1 delay time for a given sample. However, this does not represent a fundamental limitation to including greater numbers of samples and detection circuits in a probe, since modern NMR spectrometers readily accommodate additional receivers. An optimum multi-receiver configuration may consist, for example, of two or three multiplexed samples per receiver. Considering the reduced costs associated with the lower power (1–5 W) RF amplifiers required for microcoil-based probes, the total costs associated with optimization of one spectrometer to accommodate multiple samples may be considerably lower than the cost of purchasing and maintaining a second superconducting magnet and spectrometer system. A practical limit concerning the number of samples and detection circuits that can be included in a single probe is set by the overall size of the homogeneous volume of

the magnet and by the inter-flowcell spacing required to maintain adequate spectral resolution and sample-to-sample isolation.

Conclusions

This report describes the first in a new generation of commercially-available NMR detection probes capable of analyzing multiple samples simultaneously using independent flowpaths and detection circuits. The Dual-Sample Probe accomplishes detection without the usual penalties in S/N incurred, for example, if a single (larger) detection coil is used to surround two (smaller) samples. In the DSP, each sample has its own dedicated and optimized RF microcoil and z-directed gradient coil. The resulting NMR spectra from the two samples are of quality comparable to that of a CapNMR probe designed to accommodate single samples. The loading of two samples involves use of a second injection port on a liquid handling robot and duplication of the fluidic components (pumps, valves, and flowpaths) required for sample transfer to the probe. Required modifications to the NMR spectrometer are minor, consisting of the addition of a second preamplifier module and a multiplexing signal router. Simple modification to the pulse sequences enables the coordination of multiplexed data acquisition and storage from two samples in a manner that provides differentiation for separate analysis in postprocessing. Other optional modifications, e.g. the addition of a second receiver channel on the spectrometer are shown to be generally unnecessary, but are easily accommodated. Large scale verification and structure elucidation applications such as natural product library building and dereplication and metabolomic analyses seem to be obvious candidates that could benefit from the use of this technology. Higher throughput, enhanced performance, and the increased application diversity provided by the Dual-Sample Probe bring new value to existing NMR magnets and spectrometers.

Supplementary Material

Refer to Web version on PubMed Central for supplementary material.

Acknowledgments

Protasis acknowledges the financial support of the National Institutes of Health (NIH RR16387) in the development of Multi-Sample Probe technology. We also thank the School of Chemical Sciences at the University of Illinois for access to the staff and facilities of the NMR lab.

References

1. Jacobsen, N. NMR Spectroscopy Explained. John Wiley & Sons; Hoboken: 2007.
2. Lacey M, Subramanian R, Olson D, Webb A, Sweedler J. Chem Rev 1999;99:3133–3152. [PubMed: 11749512]
3. Webb A. Prog NMR Spect 1997;31:1–42.
4. Glauser G, Guillarme D, Grata E, Boccard J, Thiocone A, Carrupt PA, Veuthey JL, Rudaz S, Wolfender JL. J Chrom A 2008;1180:90–98.
5. Glauser G, Boccard J, Rudaz S, Wolfender JL. Phytochem Anal 2010;21:95–101. [PubMed: 19743069]
6. Trygg J, Holmes E, Lundstedt T. J Proteome Res 2007;6:469–479. [PubMed: 17269704]
7. Keyes P, Hernandez G, Cianchetta G, Robinson J, Lefebvre B. Magn Reson Chem 2009;47:38–52. [PubMed: 18991323]
8. Golotvin S, Vodopianov E, Pol R, Lefebvre B, Williams A, Rutkowske R, Spitzer T. Magn Reson Chem 2007;45:803–813. [PubMed: 17694570]
9. Lang G, Mayhudin N, Maya M, Sun L, van der Sar S, Blunt J, Cole A, Ellis G, Laatsch H, Monro M. J Nat Prod 2008;71:1595–1599. [PubMed: 18710284]
10. Olson D, Peck T, Webb A, Magin R, Sweedler J. Science 1995;270:1967–1970.

11. Olson D, Norcross J, O'Neil-Johnson M, Molitor P, Detlefsen D, Wilson A, Peck T. Anal Chem 2004;76:2966–2974. [PubMed: 15144211]
12. Kc R, Henry I, Park G, Raftery D. J Mag Reson 2009;197:186–192.
13. Fisher G, Petucci C, MacNamara E, Raftery D. J Magn Reson 1999;138:160–163. [PubMed: 10329239]
14. Zhang X, Sweeder J, Webb A. J Magn Reson 2001;153:254–258. [PubMed: 11740902]
15. Jayawickrama D, Sweedler J. Anal Chem 2004;76:4894–4900. [PubMed: 15307803]
16. Hou T, MacNamara E, Raftery D. Anal Chim Acta 1999;400:297–305.
17. Li Y, Wolters A, Malawey P, Sweedler J, Webb A. Anal Chem 1999;71:4815–4820. [PubMed: 10565273]
18. MacNamara E, Hou T, Fisher G, Williams S, Raftery D. Anal Chim Acta 1999;397:9–16.
19. Macnaughtan M, Hou T, Xu J, Raftery D. Anal Chem 2003;75:5116–5123. [PubMed: 14708785]
20. Wolters A, Jayawickrama D, Webb A, Sweedler J. Anal Chem 2002;74:5550–5555. [PubMed: 12433087]
21. Wang H, Ciobanu L, Edison A, Webb A. J Magn Reson 2004;170:206–212. [PubMed: 15388082]
22. Hou T, Smith J, MacNamara E, Macnaughtan M, Raftery D. Anal Chem 2001;73:2541–2546. [PubMed: 11403297]
23. Macnaughtan M, Smith A, Goldsbrough P, Santini R, Raftery D. Anal Bioanal Chem 2004;378:1520–1527. [PubMed: 15214412]
24. Lang G, Mayhudin N, Maya M, Sun L, van der Sar S, Blunt J, Cole A, Ellis G, Laatsch H, Monro M. J Nat Prod 2008;71:1595–1599. [PubMed: 18710284]

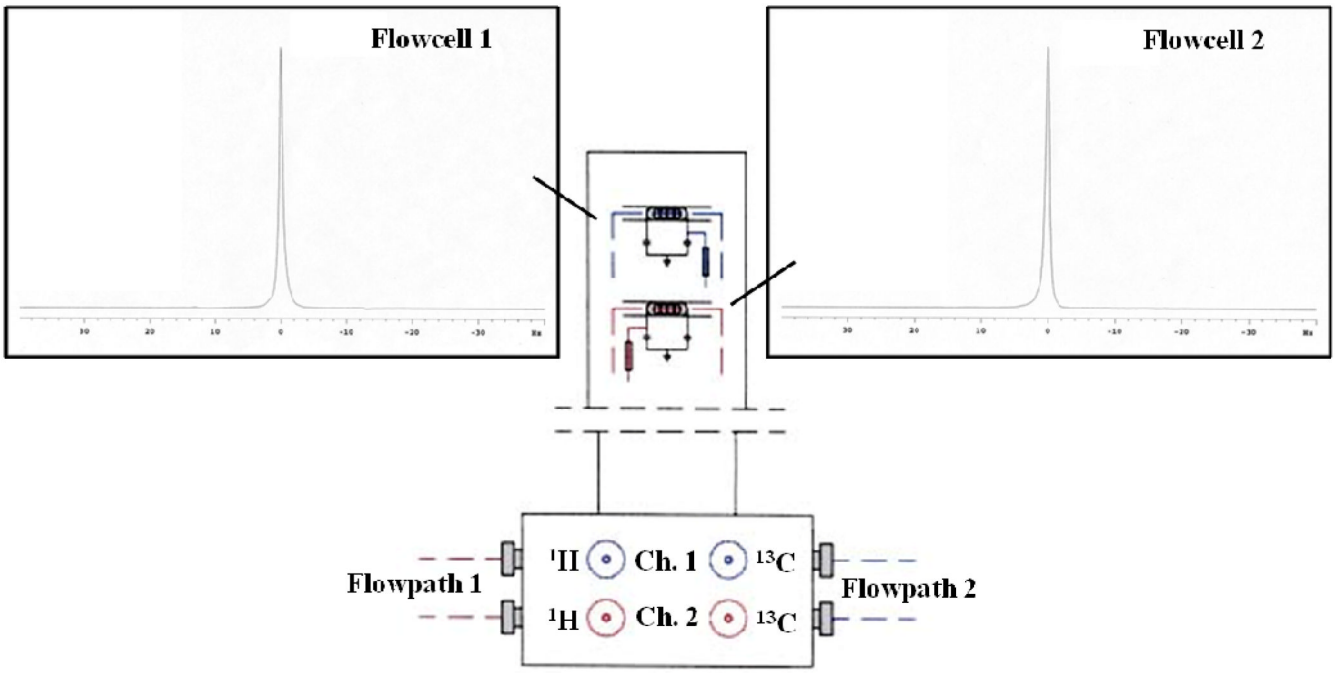

Figure 1.

Two detection circuits are incorporated into the Dual-Sample Probe to effectively provide the functionality of two probes in a single package. Although not specified in the figure, the coils are oriented orthogonally to minimize RF coupling. Both circuits are designed for $^{1}H\{^{13}C\}$ detection, and both include separate z-directed magnetic field gradient coils. The lower detection circuit provides ^{2}H field-frequency lock. Repeated in Figure S1 of the Supporting Information, the spectra shown represent two individual 5% $CHCl_3$ in DMSO-d_6 samples shimmed simultaneously (using a single set of shim values). Achieved resolutions of 0.63/6.9/12.7 Hz (upper sample) and 0.74/6.5/9.1 Hz (lower sample) were recorded for the 50/0.55/0.11% line widths and compare favorably with single-sample CapNMR probe resolution specifications.

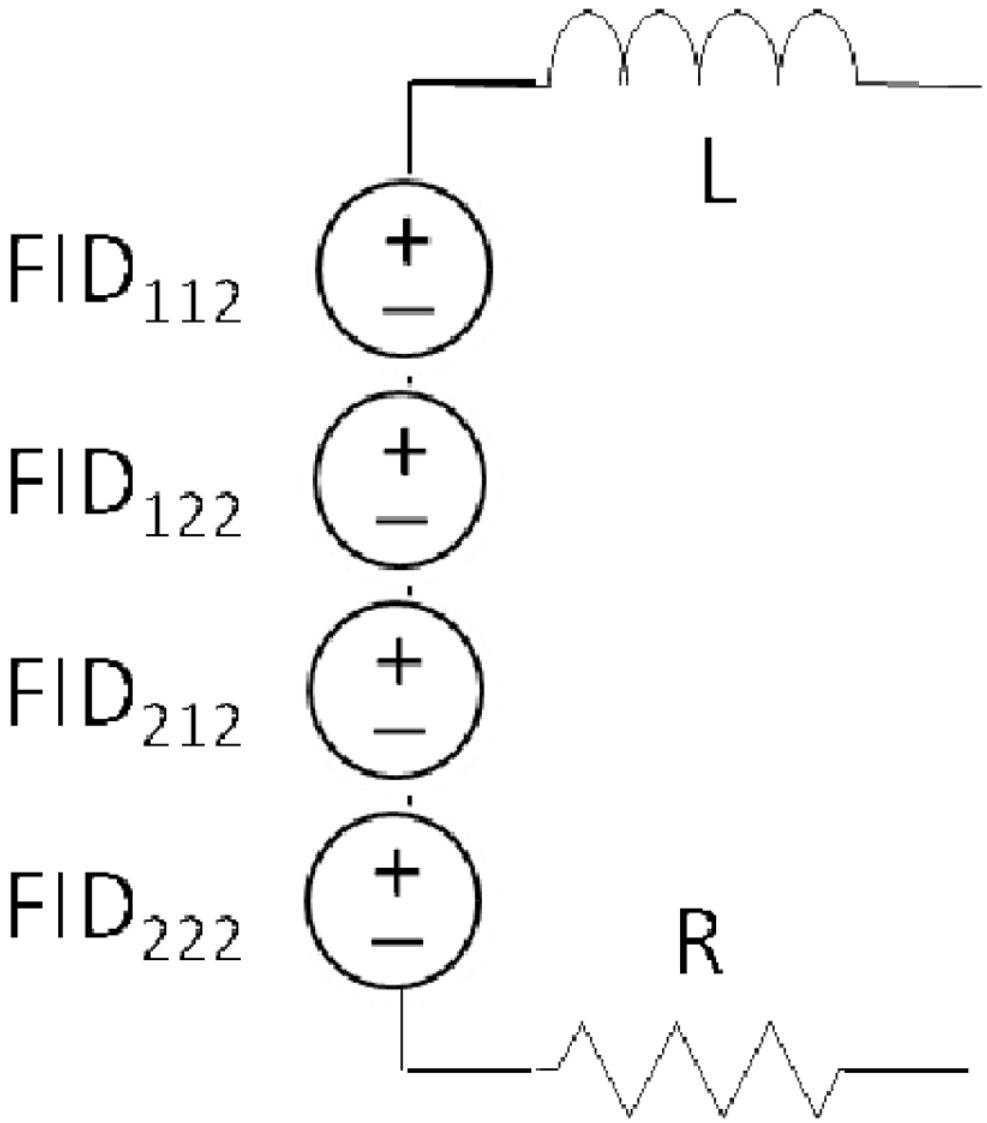

Figure 2.

Equivalent circuit model for assessment of isolation between the two samples and detection circuits of the Dual-Sample Probe. FID_{xyz} corresponds to the FID magnetization from sample × due to excitation of microcoil y and signal reception by microcoil z. Therefore, the model shown above relates specifically to the coupling as measured by the lower microcoil (#2).

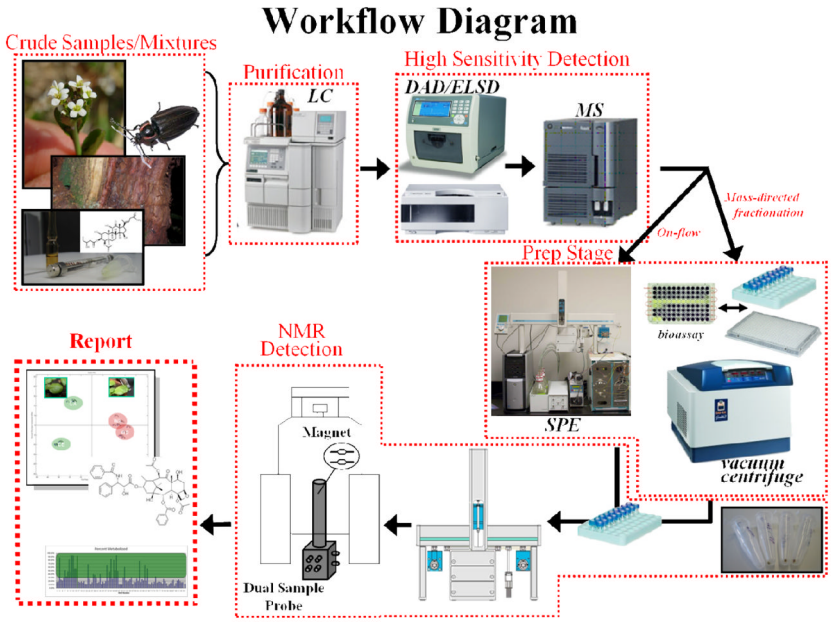

Figure 3.

Upstream sample purification, typically accomplished using high-performance liquid chromatography (HPLC), is controlled via a complement of high-sensitivity detectors in direct or indirect fluidic hyphenation. Solvent exchange and sample concentration are typically accomplished using vacuum centrifugation or solid phase extraction.

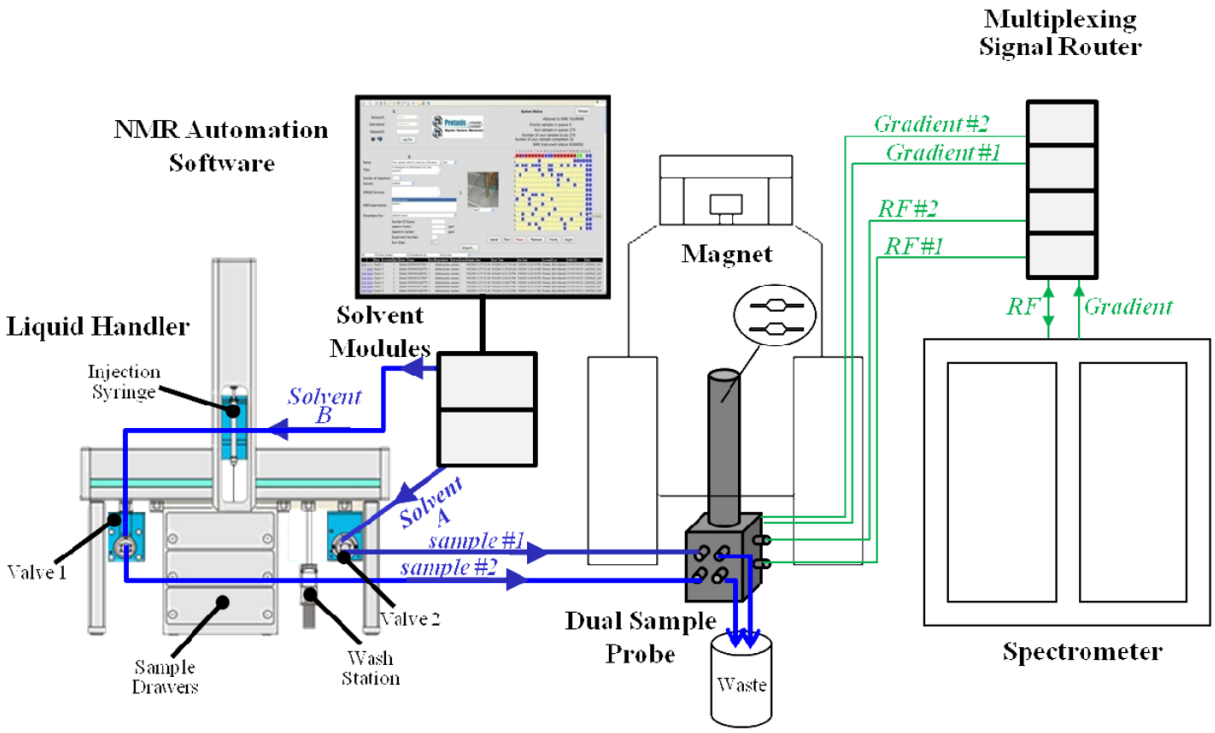

Figure 4.

System configuration for interface of the Dual-Sample Probe to an NMR spectrometer. Feedback control sensors enable robotic-based sample loading and preventive maintenance operations to ensure data quality. Barcode techniques provide import of sample information, and email reports provide easy data visualization and entry into electronic notebooks.

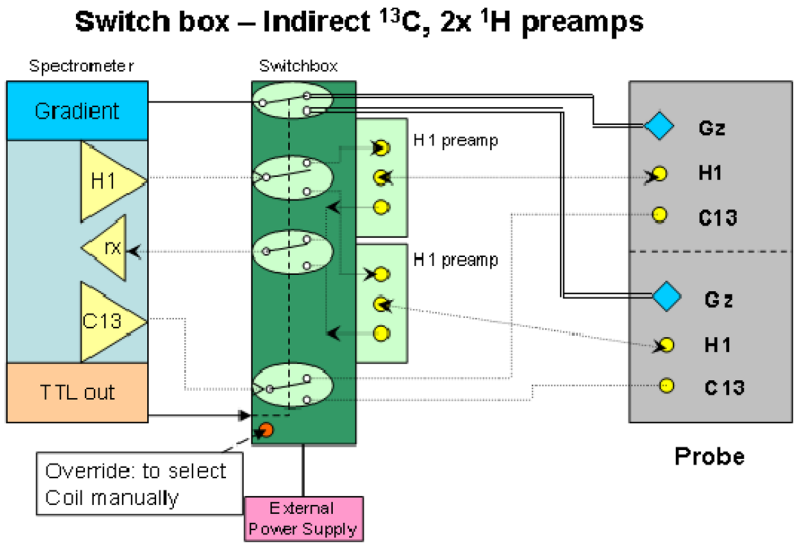

Figure 5.

A multiplexing signal router interfaces the Dual-Sample NMR Probe to conventional (single transceiver) spectrometers and provides correct signal routing. The electronic components are functionally represented in this block diagram as radiofrequency switches. Proton transmit power is routed by one switch to the appropriate preamplifier module, and subsequently delivered to the appropriate coil. Similarly, FIDs originating in one coil are cabled directly to the appropriate preamplifier, and the signal is then routed via RF switch to the spectrometer receiver. The configuration above represents proton or indirect carbon detection, but the concepts employed are amenable to replication for direct carbon detection or detection of other nuclei.

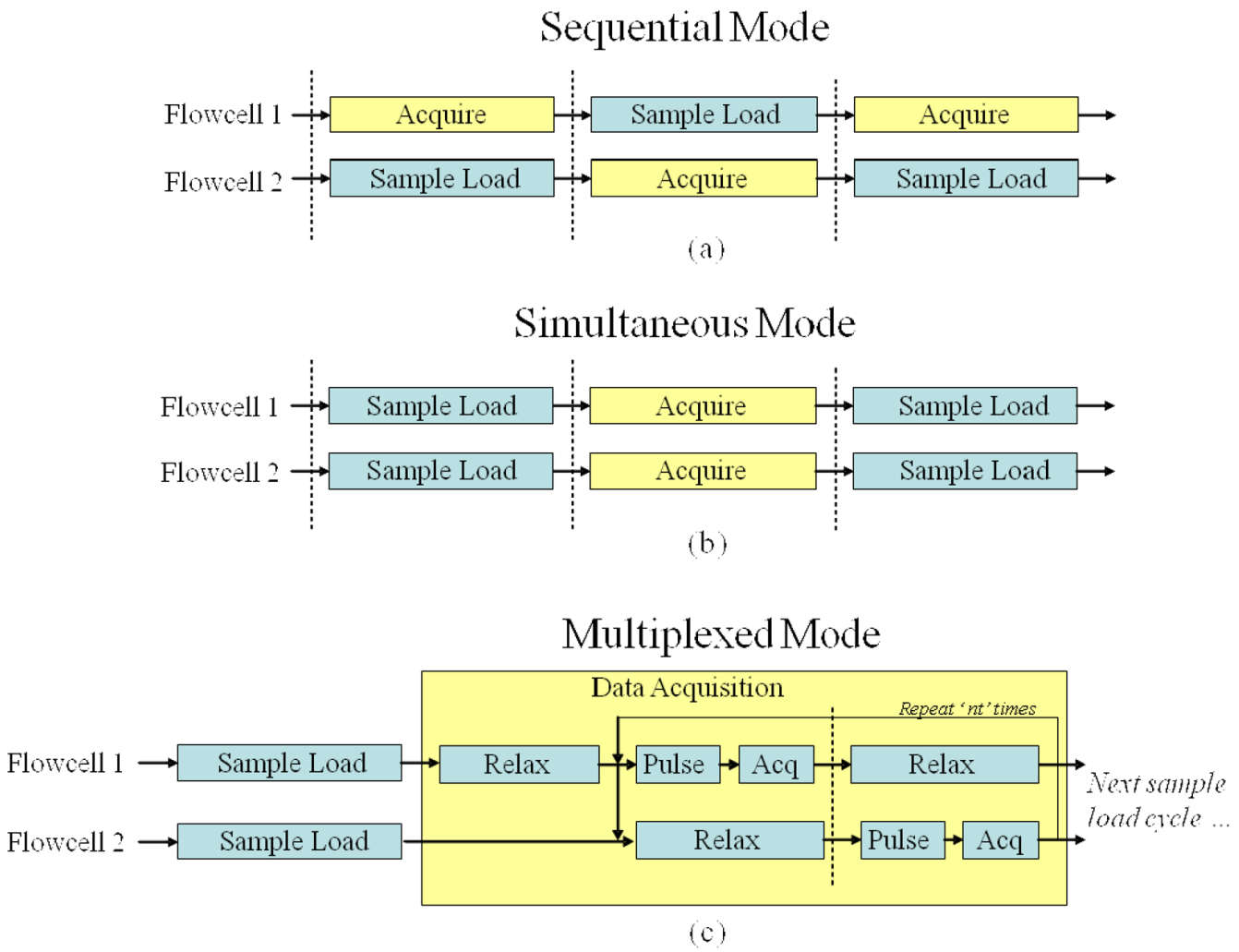

Figure 6.

Data acquisition modes for operation of the Dual-Sample Probe. (a) In sequential acquisition, sample #1 resides in flowcell #1 and is undergoing NMR data acquisition while sample #2 is loaded into flowcell #2. The process alternates as shown. Individual shim settings are stored for each detection circuit and recalled when that circuit is activated for NMR data acquisition. (b) In simultaneous acquisition, two samples are simultaneously loaded into two different flowcells, followed by data collection from each sample simultaneously. Duplicate NMR transceiver and gradient control circuitry is required. (c) The multiplexed mode of acquisition takes advantage of (T_1) sample relaxation time to multiplex the receiver path between the two samples and detection circuits. This enables use of a conventional (single transceiver and gradient control) spectrometer. In both (b) and (c) it is assumed that the same experiment is being conducted on both samples. Truly independent control with arbitrary simultaneous experiments is possible but requires modifications to spectrometer hardware and software and is not currently employed.

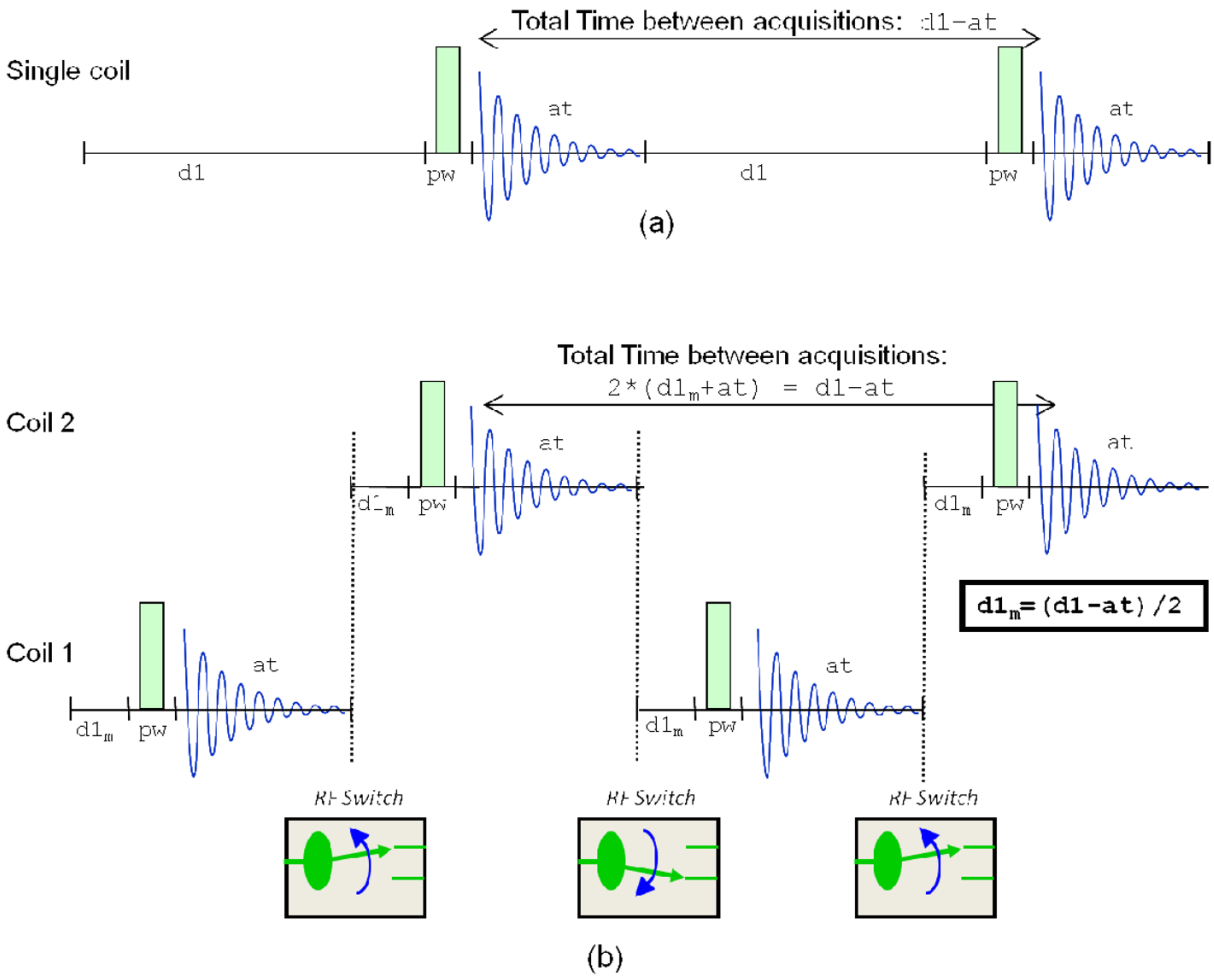

Figure 7.

Multiplexed acquisition of the FID signals from two independent samples makes productive use of the T_1 relaxation required by NMR (represented by the sequence period d1) to restore the Boltzmann distribution of spin polarization. (a) Traditional "single sample" 1D proton pulse sequence. (b) Modified Dual-Sample Probe, 1D proton pulse sequence.

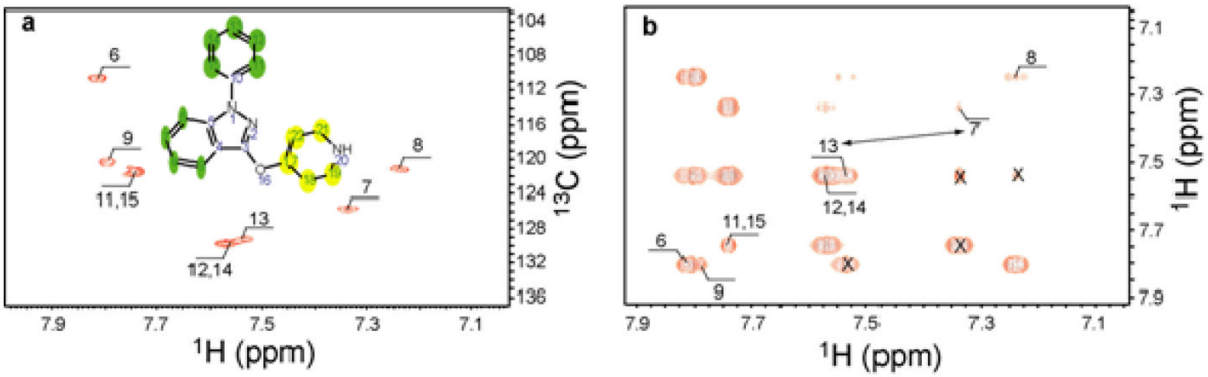

Figure 8.

Assignment retrieved from ^{1}H and HSQC combined verification (a) is not consistent with Hadamard TOCSY (b). The atoms in the structure are colored based on match factors of ^{13}C chemical shifts. Assignments of the four symmetric TOCSY off-diagonal peaks, denoted by symbol x, conflict with the coupling pattern predicted from the structure. The confliction is resolved if the assignments for atom 7 and 13 are swapped, as indicated by the arrow.

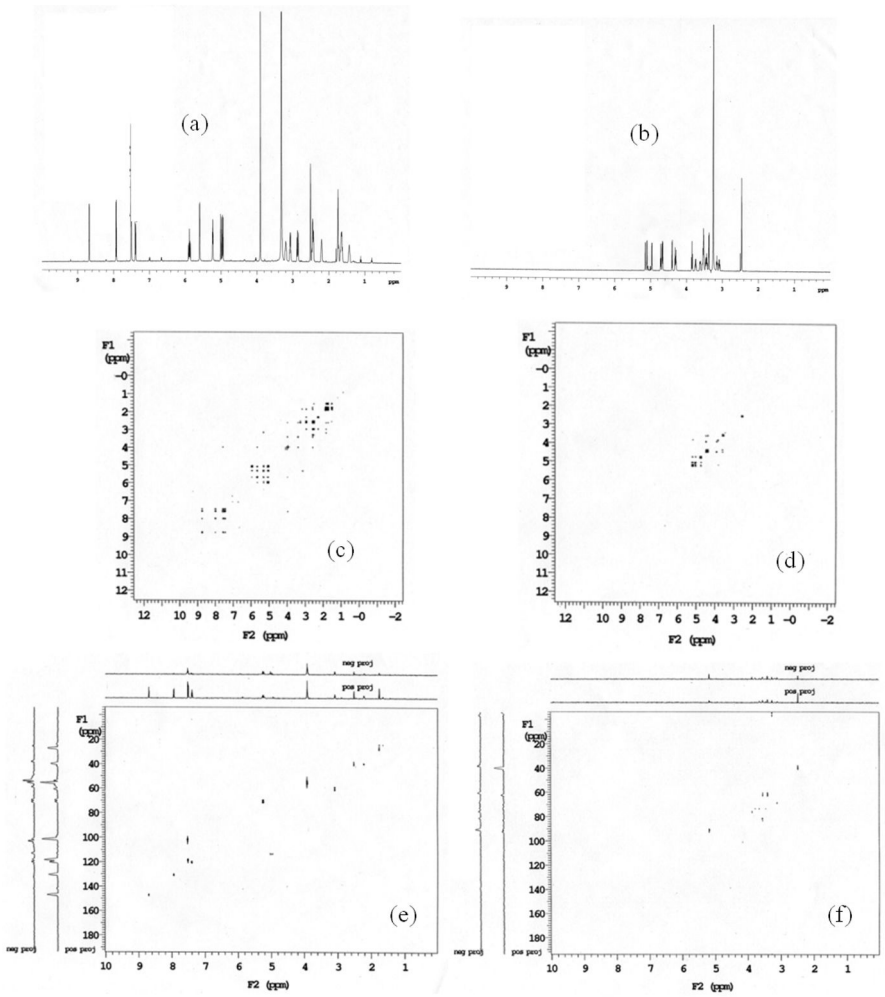

Figure 9.

NMR spectra collected using the Dual-Sample Probe operating in Multiplexed Acquisition Mode (Figure 6(c)). The lower flowcell (spectra (a), (c), and (e)) was filled with 30 mM quinine in DMSO-d_6. The upper flowcell (spectra (b), (d), and (f)) was filled with 10 mM sucrose in DMSO-d_6. Datasets (a) and (b) correspond to 1D (^{1}H) spectra, datasets (c) and (d) are 2D homonuclear (^{1}H) gradient COSY spectra, and datasets (e) and (f) are heteronuclear (^{1}H $\{^{13}$C$\}$) gradient HSQC spectra. Total acquisition times (to acquire both spectra) were 1 min, 7 s (16 scans/sample) for the 1D spectra ((a), (b)), 6 min, 6 s (4 transients, 64 increments) for the g-COSY spectra ((c), (d)), and 28 min, 48 s (8 transients, 100 increments) for the g-HSQC spectra ((e), (f)).

Table 1

Measured Coupling Coefficients. The equivalent coefficients for the circuit model of Figure 2 are indicated in the right-most column.

Coupling Coefficient (measured)	Value (%)	Value (dB)	Error Type	Equivalent Coefficients (Model of Figure 2)
F_{112}	1.5 %	−36 dB	Quantitation	F_{112}
F_{121}	2 %	−34 dB	Impurity	F_{212}
F_{122}	0.04%	−68 dB	Impurity	F_{122}